Biosensors and Bioelectronics 149 (2020) 111840

Contents lists available at ScienceDirect

Biosensors and Bioelectronics

journal homepage: http://www.elsevier.com/locate/bios

A simple aptasensor for $A\beta_{40}$ oligomers based on tunable mismatched base pairs of dsDNA and graphene oxide

Yana Zhao [a,1], Xin Li [b,1], Yuan Yang [c], Shihui Si [a], Chunyan Deng [a,*], Huiyun Wu [b,**]

[a] College of Chemistry and Chemical Engineering, Central South University, Changsha, 410083, China
[b] Academy of Military Medical Sciences, Academy of Military Sciences, Beijing, 100850, China
[c] Institute of Biomaterials and Biomedical Engineering, University of Toronto, Toronto, Ontario, M5S 3G9, Canada

ARTICLE INFO

Keywords:
β-amyloid 1–40 oligomers ($A\beta_{40}O$)
Graphene oxide (GO)
Aptasensor
Mismatch

ABSTRACT

β-amyloid 1–40 oligomers ($A\beta_{40}O$) is considered to be one of the important biomarkers for the diagnosis and treatment of Alzheimer's disease (AD). To explore a method with excellent performance is favorable for measuring the low concentration of $A\beta_{40}O$ in AD patients. Here, we developed a simple and fast method with a double stranded DNA (dsDNA)/graphene oxide (GO) based sensor, which was a fluorescent probe for a highly sensitive detection of $A\beta_{40}O$ down to 0.1 nM with a linear detectable range from 0.1 nM to 40 nM. The proposed sensor effectively reduced non-specific adsorption and improved the specificity of detection because of the covalent conjugation of a binding DNA (bDNA) containing $A\beta_{40}O$-targeting aptamer ($Apt_{A\beta}$) onto GO surface, as well as the optimization of the number of mismatch base pairs of dsDNA. Moreover, AD patients and healthy persons were distinguished by this present method. All advantages of this method are exactly what the clinical detection of AD biomarkers need. This novel aptasensor might pave a way towards the early diagnosis of AD.

1. Introduction

Alzheimer's disease (AD) is a dementia caused by chronic progressive central nervous system degeneration, with a high prevalence in the elderly. It's mainly characterized by neuropsychiatric symptoms such as progressive memory impairment, cognitive dysfunction, personality changes, and speech disorders (Hallikainen et al., 2012; Stopschinski and Diamond, 2017). Neuropathological studies have confirmed that extracellular senile plaque deposition, intracellular accumulation of neurofibrillary tangles and neuronal degeneration loss are the main pathological hallmarks of AD (Perrin et al., 2009; Jakob-Roetne and Jacobsen, 2009). At present, there is no curative treatment of AD, although various therapeutic strategies were evaluated (Englund et al., 2007; Mroczko et al., 2018). Therefore, the early diagnosis, conducting before clinical symptoms shown, is crucial and essential for AD treatment. To measure the reliable biomarkers of AD is one of the efficient methods of early diagnosis (Englund et al., 2007).

amyloid-β (Aβ) peptides are major components of senile plaque (Yamada et al., 1999; Fukuta et al., 2001), which are important biomarkers for diagnosis of AD (Hanson et al., 2006; Mroczko et al., 2018). But it also presents in cerebrospinal fluid (CSF) at a very low concentration (in subnanomolar level) (Xia et al., 2010). It was reported that Aβ oligomeric species (AβOs) were the main toxic species in human CSF, which generally accumulate at a very early stage of the disease acting as the first indicator of AD (Small and Cappai, 2006; Taylor et al., 2010; Mroczko et al., 2018). Xia et al. suggested that the levels of AβOs might increase with the disease progressing (Xia et al., 2009; Yang et al., 2017). Although there are no reports about the AβO levels at different stages of AD, it can be deduced that the level of AβOs is also very low in CSF according to the low concentration of Aβ in CSF. Therefore, the high sensitivity is required to detect the low concentration AβO. So far, numerous methods have been explored aiming to measure AβOs such as enzyme-linked immunosorbent assay (ELISA) (Xia et al., 2009; Bruggink et al., 2013), surface plasmon resonance (SPR) (Yi et al., 2015), surface-enhanced Raman spectroscopy (SERS) (Guerrini et al., 2015) and electrochemical method (Rushworth et al., 2014; Felismina et al., 2017), which were generally complex-constructed and required instrument-professionals. Especially they were mostly antibody-based, which often suffered from the disadvantages such as cross-reactivity, high non-specific binding (Mukhopadhyay, 2005; Taylor and Freed,

* Corresponding author.
** Corresponding author.
E-mail addresses: dengchunyan@csu.edu.cn (C. Deng), Huiyunwu740@126.com (H. Wu).
[1] Equally contributed to this work.

https://doi.org/10.1016/j.bios.2019.111840
Received 21 May 2019; Received in revised form 30 October 2019; Accepted 1 November 2019
Available online 4 November 2019

1976), relatively expensive and poor stability, resulting in time-consuming and low specific detection of AβOs. Moreover, the sensitivities of most reported methods were not capable to meet this requirement for the low AβO concentration (Liu et al., 2017; Mukhopadhyay, 2005). Up to now, there is a lack of an inexpensive, sensitive, and specific detection strategy for the AβO detection (Englund et al., 2007; Mroczko et al., 2018). It is necessary to develop a novel AβO biosensor that is ultrasensitive, simple, cost-effective, fast and more applicable, providing an efficient diagnostic method of practical use in clinical application.

One hand, aptamers-based sensing devices have been widely developed for molecular analysis and medical diagnostics (Zhao et al., 2018; Baker et al., 2006; Xiao et al., 2005; Deng et al., 2018) due to their high sensitivity and accurate specificity. Aptamers can be used as emerging recognition-binding molecules instead of antibodies because they possess such advantages as ease of synthesis and reproducibility, lack of immunogenicity, chemical stability, low molecular weight, design versatility (Ellington and Szostak, 1990; Robertson and Joyce, 1990; Deng et al., 2009), and also specifically bind to various targets. Therefore, using aptamer as recognizing receptors to develop biosensors for AβOs can be expected to be useful and effective to improve the performance of AβO-sensing biosensors.

On the other hand, analytical methods employed for aptasenor are also very important for the design of clinical application. Various methods including electrochemistry, SPR, ELS, Raman, fluorescence and colorimetery have been developed. Among them, fluorescence technology as a convenient analytical tool for molecular recognition and biomedical diagnosis has been attracted much interest in target analysis due to its inherent ease of operation and high sensitivity (Lu et al., 2017). In recent years, various work about graphene oxide (GO)-based fluorescent aptasensors have been reported (He et al., 2010, 2012; Chang et al., 2010; Huang et al., 2015) because GO possesses excellent fluorescence quenching ability and can strongly adsorb single-stranded DNA (ssDNA) (Swathi and Sebastian, 2009). For these aptasensors, aptamers were physically adsorbed on GO surface, which generally caused the adsorbed probe to be displaced by a non-target molecule, thus generating a false positive signal (Liu et al., 2014). To overcome this disadvantage, Liu et al. proposed to immobilize ssDNA onto GO surface by covalent binding, and achieving the highly specific detection of targets. It has been proved that this method for immobilization of ssDNA onto GO surface is useful for improving the specificity, reproducibility and accuracy of GO-based fluorescent aptasensor (Liu et al., 2014). Until now, the fluorescent methods for AβOs detection have rarely been reported. Hence, to develop fluorescent biosensors for AβOs may pave the way to develop a new diagnostic device for the early diagnosis of AD.

Considering the importance and challenge of AβOs detection, especially the detection sensitivity of $A\beta_{40}O$ is crucial for the detection of the low $A\beta_{40}O$ concentration in CSF. Herein we developed a simple and sensitive method for $A\beta_{40}$ oligomer ($A\beta_{40}O$) detection of low concentration based on GO and tunable mismatched base pairs of dsDNA. $A\beta_{40}O$-binding aptamer ($Apt_{A\beta}$) modified with FAM at 5′ end and amino group (NH_2-) at 3' end was noted as binding DNA (bDNA). cDNAs were designed to be complementary to bDNA. dsDNA was formed through the hybridization of bDNA and cDNA. The resultant dsDNA/GO was used as a fluorescent sensing device for $A\beta_{40}O$ detection. In the absence of $A\beta_{40}O$, FAM was away from GO surface because of the rigidity of dsDNA, and therefore the fluorescent signal of dsDNA/GO was obvious. Introducing $A\beta_{40}O$, the specific binding of $A\beta_{40}O$ to $Apt_{A\beta}$ occurred, which led to $Apt_{A\beta}$ folding and FAM approaching GO surface. The fluorescence of FAM was quenched by GO, resulting in the decrease of fluorescence signal. Based on mechanism described above, the detection of $A\beta_{40}O$ was feasible. Moreover, the detection sensitivity of this novel biosensor was improved by optimizing the number of mismatched base pairs of dsDNA, leading to the quantitative detection of $A\beta_{40}O$ of a wider linear range and lower detectable concentration compared to the conventional methods. The detectable lowest concentration of 0.1 nM was achieved. Additionally, high specificity has been achieved because of the covalent immobilization of $Apt_{A\beta}$. This proposed strategy is not only simple and cost effective, but also highly sensitive, specific and rapid, which may expand its applications in biomedical field.

2. Experimental section

2.1. Materials and instruments

The bDNA and cDNAs used in this work were purchased from Shanghai Sangon Biotechnology Co., Ltd. (Shanghai, China), and their sequences and names were listed in Table S1. Graphite powders (325 mesh) with purity of 99.95% were obtained from Aladdin (Shanghai, China). NaCl, $MgCl_2$, 4-(2-Hydroxyethyl)-piperazine-1-ethanesulfonic acid (HEPES), N-(3-Dimethylaminopropyl)-N′-ethylcarbodiimide hydrochloride (EDC), N-Hydroxysuccinimide (NHS) were purchased from Sigma (Shanghai, China). $A\beta_{40}$ and $A\beta_{42}$ peptides were provided by Xinghao medicine Co., Ltd (Wuhan, China). Other regents were purchased from Beijing Chemical Company (China). Artificial cerebrospinal fluid (ACSF) was prepared from 140 mM NaCl, 20 mM KCl, 1 mM MgCl, 1 mM $CaCl_2$, 5 mM HEPES, and 10 mM glucose (Yin et al., 2019). Unless otherwise noted, all other chemicals were analytical grade purity and used without further purification. All of prepared solutions were stored at 4 °C as stock solution. Milli-Q water (Millipore M-Q system Inc., 18.2 MΩ cm) was used in all experiments.

Fluorescent emission spectra were performed on a FL-4600 fluorescence spectrophotometer (Hitachi High-Technology Co., Ltd, Tokyo, Japan). X-ray photoelectron spectroscopy (XPS) analysis was carried on K-Alpha$^+$ model X-ray Photoelectron Spectroscopy (Thermo fisher Scientific). FT-IR spectra were performed by attenuated total reflectance (ATR) in the range of 400–4400 cm^{-1}, with 4 cm^{-1} resolution using an Agilent Technologies Cary 630 spectrometer. UV–visible (UV–vis) spectra were monitored using a UV-2450 spectrophotometer (Shimadzu, Kyoto, Japan).

2.2. Synthesis of graphene oxide

GO was synthesized from graphite powder based on the Hummer's method (Hummers and Offeman, 1958). In brief, 2.5 g graphite powder and 1.25 g sodium nitrate were dissolved in 55 mL concentrated sulfuric acid in an ice-bath. Under continuous stirring, 7.5 g $KMnO_4$ was carefully added to keep the suspension temperature under 20 °C. Then, the ice-bath was removed, and the mixed solution was stirred for 30 min. Subsequently, 110 mL deionized water was slowly added into the solution, the temperature rapidly increased. After 15 min, 25 mL of 30% H_2O_2 was added to remove excess $KMnO_4$ and the solution turned bright yellow. Finally, the prepared GO was washed several times with 5% HCl and deionized water, then suspended at a concentration of 10 mg mL^{-1} for later use.

2.3. Preparation of $A\beta_{40}O$

The preparation of $A\beta_{40}O$ was carried out according to previous reports in literature (Geng et al., 2011; Deng et al., 2018). Briefly, $A\beta_{40}$ powder was dissolved in HFIP at a concentration of 1 mg mL^{-1} and incubated overnight at 4 °C in a refrigerator. Subsequently, the solution was sonicated for 30 min at low temperature, and then lyophilized in a freeze dryer (Virtis Bendtop K, SP scientific Gardiner, NY). The obtained lyophilized powder was dissolved in HEPES (25 mM, pH 7.6), and incubated for 3 days in thermostatic water bath at 37 °C to obtain $A\beta_{40}O$. The $A\beta_{40}O$ solution was then filtered through a Millipore YM-30 membrane for further use. The concentration of $A\beta_{40}O$ solution was measured by UV–vis spectra peak of tyrosine at 276 nm ($\varepsilon = 1410\ M^{-1}\ cm^{-1}$).

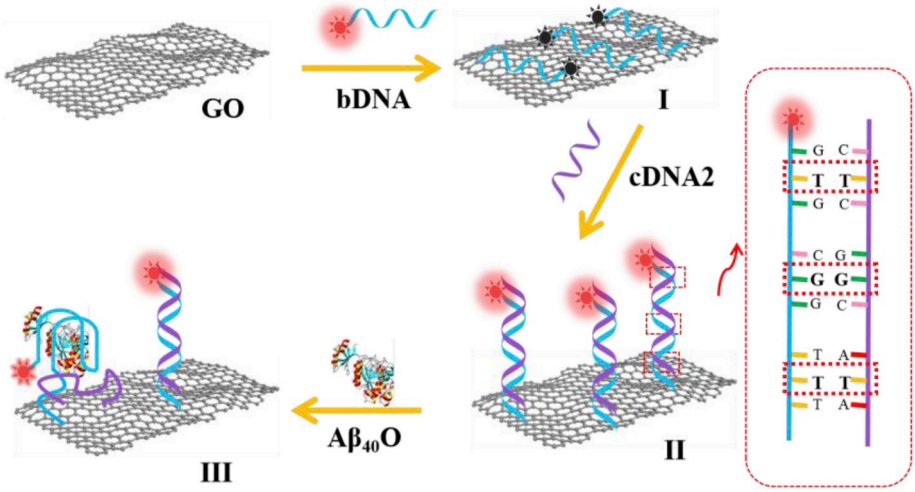

Scheme 1. Schematic illustration of the dsDNA2/GO-based fluorescence sensor for $A\beta_{40}O$ detection. (I) the bDNA was covalently bound onto the surface of GO to form bDNA/GO; (II) the cDNA2 was hybridized with bDNA to achieve dsDNA modified GO (dsDNA/GO); (III) The dsDNA/GO after incubated with $A\beta_{40}O$.

2.4. Construction of sensor

GO (1 mg mL^{-1}) was sonicated for 20 min to obtain uniformly dispersed sheet structure, which was quantified with an absorption peak at 228 nm by UV–vis spectra (Yu et al., 2018). In a typical experiment, GO solution (1 mg mL^{-1}, 100 μL) was mixed with EDC (25 mM, 40 μL), NHS (25 mM, 20 μL) and bDNA (4 μM, 50 μL), then deionized water was added to a final volume of 400 μL. The mixture was continuously shook for 3 h at room temperature in the dark. Then the solution was centrifuged at 14000 rpm for 15 min followed by removing the supernatant, and washed with 400 μL of deionized water for 3 times to further remove non-covalently linked DNA. The bDNA/GO solution was prepared.

Subsequently, the bDNA/GO solution was then incubated with 50 μL, 12 μM cDNAs for 2 h to achieve the hybridization between cDNAs and bDNA. Afterward, the obtained solution were centrifuged at 14000 rpm for 15 min and washed several times. Finally, the precipitate was dispersed in HEPES buffer to obtain the dsDNA/GO solution, which was stored at 4 °C for further use. Herein, in order to optimize the performance of this proposed biosensor for $A\beta_{40}O$, different cDNAs were designed and employed to fabricate different dsDNA/GO, which were denoted as dsDNA1/GO, dsDNA2/GO, dsDNA3/GO, dsDNA4/GO and dsDNA5/GO, respectively (see Table S1 for detail).

2.5. Sensor testing

Firstly, initial signals of dsDNA/GO solutions were monitored. Then, a series of $A\beta_{40}O$ solutions with different concentrations were added to dsDNA/GO solutions, and incubated for 30 min in a thermostatic water bath. Afterward, the fluorescence emission spectra of the mixture were recorded at 520 nm. For control experiments, different interfering protein solutions were employed to be incubated with dsDNA/GO solutions under the same conditions, and then the fluorescence intensities were also measured.

2.6. Preparation of CSF samples

The CSF samples from AD patients and healthy persons were provided by the Third Xiangya Hospital of Central South University, respectively. These real CSF samples were collected by lumbar puncture using a 22-gauge Quincke-type needle, aliquoted, and stored at −80 °C. To reduce the disturbance from co-existing Aβ aggregates (larger oligomers and fibrils) and other proteins, CSF samples were filtrated with a Millipore YM-30 membrane before the measurement.

3. Results and discussion

3.1. Design strategy

Scheme 1 shows fabrication of the fluorescent sensor and the sensing mechanism for $A\beta_{40}O$. In this strategy, bDNA, cDNAs and GO are involved. $Apt_{A\beta}$ is employed as recognition receptors and FAM serves as signal probe for the determination of $A\beta_{40}O$. bDNA is covalently bound to GO at first (Scheme 1-I), and then the hybridization between bDNA and cDNA is carried out to achieve the dsDNA modified GO (dsDNA/GO) (Scheme 1-II). In this case, the rigidity of dsDNA causes the bound bDNA stretching, and therefore the fluorophore FAM is away from GO surface. Correspondingly, the fluorescent signal (F_0) of dsDNA/GO is visualized. However, upon the incubation of $A\beta_{40}O$, the specific binding of $A\beta_{40}O$ to $Apt_{A\beta}$ leads to the separation of cDNA from dsDNA, causing FAM approaching to GO surface because of the $Apt_{A\beta}$'s folding (Scheme 1-III). Subsequently, FAM's fluorescence is quenched, resulting in its fluorescent signal F. The quantitative detection of $A\beta_{40}O$ can be realized based on the relative fluorescence intensity (1-F/F_0).

In this strategy, this proposed dsDNA/GO-based aptasensor is expected to possess excellent performance because of the following reasons: (1) The sensor is simple to construct for achieving the analysis of target; (2) we try to employ different cDNAs to change the number of mismatched base pairs between cDNA and bDNA to obtain a high sensitivity, which is useful to measure the low concentration of $A\beta_{40}O$; (3) $Apt_{A\beta}$ is covalently linked to GO surface, which improves the detection specificity. This work provides a simple, high specific and sensitive method for the detection of $A\beta_{40}O$, exhibiting the excellent sensing performance.

3.2. Characterization of GO and dsDNA/GO

The XPS spectrum was used to characterized the elemental composition and types of chemical bonds of GO. As shown in Figs. S1–A, C1s peak spectrum of GO was subjected to peak fitting to obtain three components, and the three components corresponded to carbon atoms in different functional groups: C (BE, 284.84 eV) in graphite. C (BE, 286.93 eV) and carbonyl C (BE, 288.02 eV) in the CO epoxy/ether group, C1s spectrum of GO clearly showed a considerable degree of oxidation, and XPS results proved that the preparation of GO is successful.

In order to confirm the successful synthesis of dsDNA/GO, FT-IR measurement was performed. As shown in Figs. S1–B, the band at 3413 cm^{-1} was attributed to νOH, 1723 cm^{-1} band was $\nu C=O$ of

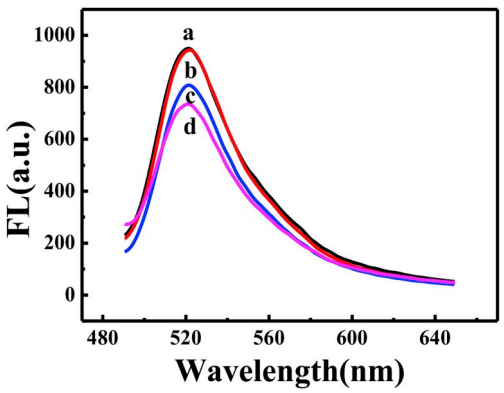

Fig. 1. Feasibility of this sensor. Fluorescent responses of the dsDNA1/GO before (curve a) and after incubated with HEPES buffer (25 mM, pH 7.6) (curve b), 30 nM (curve c), or 100 nM $A\beta_{40}O$ (curve d), respectively.

carboxylic acid and ketone groups, and 1625 cm^{-1} band was derived from $\nu C=C$. The spectrum clearly showed the band of functional groups of GO, which further indicated the successful synthesis of GO. For dsDNA/GO, the band at 1723 cm^{-1} (C═O) disappeared and a new band appeared at 1649 cm^{-1} (amide), indicating successful formation of amide bonds between GO and amino-modified $Apt_{A\beta}$. The results above demonstrated that GO and dsDNA/GO were synthesized and prepared successfully.

3.3. Feasibility of this sensor

We investigated the feasibility of this fluorescent sensor for $A\beta_{40}O$ detection. Herein, dsDNA1/GO was firstly employed to be incubated with different concentrations $A\beta_{40}O$, and the corresponding results were shown in Fig. 1. Upon dsDNA1/GO was treated with $A\beta_{40}O$, the fluorescence intensity of dsDNA1/GO decreased (curve c, d) comparing to the initial response of dsDNA1/GO (curve a). While dsDNA1/GO was incubated in HEPES buffer without $A\beta_{40}O$, the fluorescence intensity of dsDNA1/GO almost did not change (curve b). Therefore, it can be speculated that the specific binding of $A\beta_{40}O$ to $Apt_{A\beta}$ occurred based on this strategy. The formation of $A\beta_{40}O$-Apt complex caused $Apt_{A\beta}$ folding, and FAM approaching to GO surface, which resulted in FAM's fluorescence quenching obviously. This proposed strategy is feasible for the detection of $A\beta_{40}O$.

3.4. The optimization of cDNA sequence

In this strategy, the binding of $A\beta_{40}O$ to bDNA was expected to cause the separation of cDNAs from dsDNA. Therefore, the binding affinity between cDNA and bDNA was critical for the detection sensitivity of $A\beta_{40}O$. While for dsDNA, the number of matched base pairs was a key element for the binding affinity. So, we optimized the sequence of cDNA to achieve a high sensitivity for the detection $A\beta_{40}O$. Different sequenced cDNAs (as listed in Table S1) were designed and used to hybridize with bDNA/GO, based on which the background signals (F_0) of different fluorescent probes were shown in Fig. 2A. It was clearly found that F_0 of dsDNA2/GO (curve b) was the same as that of dsDNA1/GO (curve a). However, when the numbers of mismatched base pairs increased, F_0 of dsDNA3/GO (curve c), dsDNA4/GO (curve d), dsDNA5/GO (curve e) were obviously lower than those of dsDNA1/GO and dsDNA2/GO. These findings demonstrated that the number of mismatched bases in dsDNA has an important effect on F_0 of dsDNA/GO. We speculate that the rigidity of dsDNA gradually weakened as the decrease of the number of the mismatched base pairs, resulting in a decrease of the distance between FAM and GO surface and therefore a relatively low F_0. Furthermore, considering that low F_0 was unfavorable for high sensitivity of a "signal-off" sensor, cDNA1 and cDNA2 might be more suitable to construct the dsDNA/GO-based fluorescence probes.

In order to make sure the optimal performance for detection of $A\beta_{40}O$, we further investigated the response of dsDNA1/GO and dsDNA2/GO to 40 nM $A\beta_{40}O$, respectively, as shown in Fig. 2B. We found that the dsDNA2/GO's response was more obvious than that of dsDNA1/GO incubating with the same concentration of $A\beta_{40}O$, which suggested that the higher sensitivity of dsDNA2/GO to $A\beta_{40}O$ compared to the one of dsDNA1/GO even though both dsDNA1/GO and dsDNA2/GO showed almost the same level of F_0. Therefore, dsDNA2/GO is chosen as a fluorescence probe for $A\beta_{40}O$ detecting.

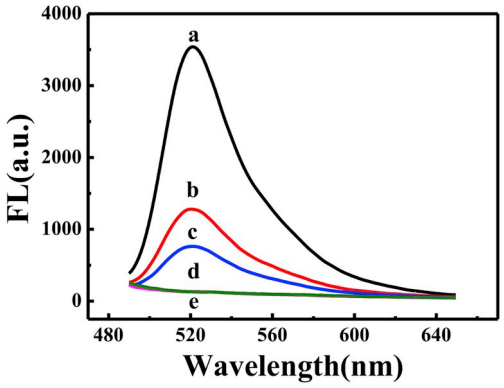

Fig. 3. Fluorescence spectra of bDNA/GO solutions. bDNA/GO solutions were obtained by incubated GO (1 mg mL^{-1}) with different concentrations of bDNA (from a to d: 10 μM (curve a), 6 μM (curve b), 4 μM (curve c), 2 μM (curve d) and 1 μM (curve e)).

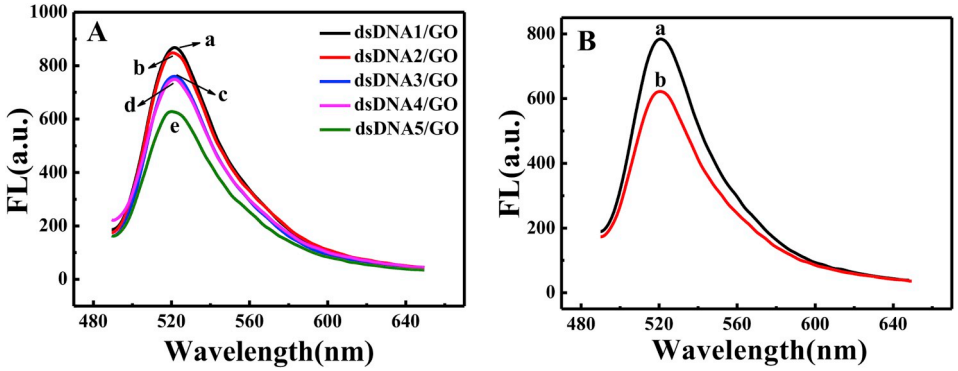

Fig. 2. (A) Initial fluorescent responses of dsDNA1/GO (curve a), dsDNA2/GO (curve b), dsDNA3/GO (curve c), dsDNA4/GO (curve d), dsDNA5/GO (curve e). (B) The fluorescent responses of the dsDNA1/GO-based senor (curve a) and dsDNA2/GO-based sensor (curve b) to 40 nM $A\beta_{40}O$, respectively.

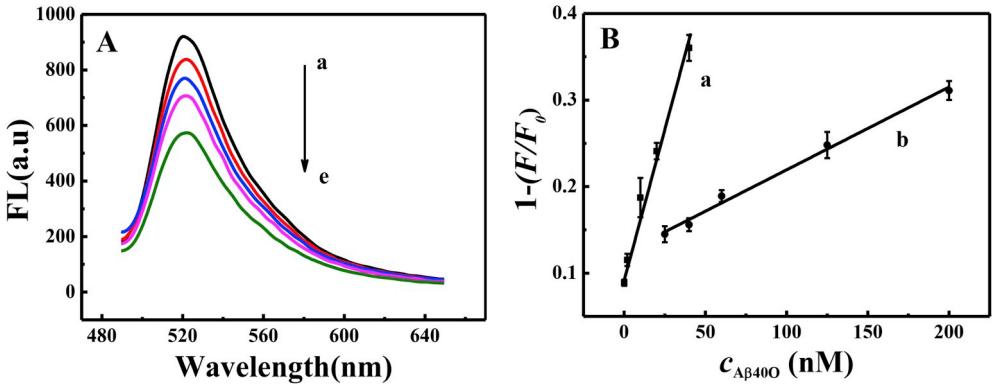

Fig. 4. (A) Fluorescence responses of dsDNA2/GO to various concentrations of $A\beta_{40}O$ (from a to e: 0, 0.1, 10, 20, 40 nM). (B) Curve a and curve b were linear relationship between 1-F/F_0 and $A\beta_{40}O$ concentrations obtained from the dsDNA2/GO-based sensor and dsDNA1/GO-based sensor, respectively. The error bars mean the standard deviation for four detections of the same concentration $A\beta_{40}O$ ($n = 4$).

3.5. Optimization of conditions

3.5.1. bDNA concentration

1 mg mL^{-1} GO was used for fabrication of probes. In order to ensure the saturated binding of bDNA to GO surface, we employed bDNA solutions with different concentrations to incubate with 1 mg mL^{-1} GO, after which the fluorescent intensities of the resultant bDNA/GO solutions were measured, as displayed in Fig. 3. It was observed that the fluorescence intensity of bDNA/GO reduced gradually as the bDNA concentration decreasing from 10 to 1 μM. Additionally, when 4 μM bDNA was incubated with 1 mg mL^{-1} GO solution, the fluorescence emission spectrum of bDNA/GO was obvious. However, when bDNA concentration was less than 2 μM, there was no fluorescence signal because of FAM's quenching by GO. As a conclusion, 4 μM bDNA was chosen as the optimal concentration, which not only prevented bDNA from wasting, but also ensured the saturated immobilization of GO by bDNA.

3.5.2. Temperature and incubation time

Temperature can affect protein's secondary structure, and subsequently influence on its interaction with aptamer. In this work, the effect of temperature on detection sensitivity was investigated and shown in Figs. S2–A. Responses (1-F/F_0) of dsDNA2/GO to 20 nM $A\beta_{40}O$ were different upon different temperature, in which the highest fluorescence intensity was observed at the reaction temperature of 25 °C, suggesting the optimal temperature was set at 25 °C favoring the specific binding of $Apt_{A\beta}$ and $A\beta_{40}O$.

In addition, incubation time for $Apt_{A\beta}$ and $A\beta_{40}O$ was another key for the biosensor's performance. We measured the fluorescence intensities of dsDNA2/GO solution in the presence of 20 nM $A\beta_{40}O$ every 5 min. As shown in Figs. S2–B, 1-F/F_0 increased with incubation time prolonging, and reached a platform when incubation time was 30 min. Therefore, 30 min was chosen as the optimal reaction time for the detection of $A\beta_{40}O$, showing a rapid response of the biosensor to targets.

3.6. Sensing $A\beta_{40}O$

Fig. 4A showed the fluorescence emission spectrum of dsDNA2/GO in the presence of different concentrations of $A\beta_{40}O$. The fluorescence intensity of dsDNA2/GO dramatically decreased with $A\beta_{40}O$ concentrations increasing from 0.1 nM to 40 nM, which further proved the feasibility of this aptasensor. The decreased fluorescent intensity was attributed to the binding of $Apt_{A\beta}$ to $A\beta_{40}O$, resulting in the fluorescence quenching followed the Stern−Volmer equation (Li et al., 2013).

$$F_0/F = 1 + K_{sv}\,[Q] \quad (1)$$

F_0 and F were the FL intensity of dsDNA2/GO-based probe in the absence and presence of $A\beta_{40}O$, respectively, K_{SV} was the Stern−Volmer constant, and [Q] was the concentration of $A\beta_{40}O$. Therefore, 1-(F/F_0) is proportional to the concentration of $A\beta_{40}O$. As shown in Fig. 4B, the linear equation was obtained as 1-(F/F_0) = 0.00709 $c_{A\beta40O}$ + 0.0914 ($R = 0.9926$). A wide linear range from 0.1 to 40 nM with the detectable lowest concentration of 0.1 nM was obtained. This aptasensor possesses higher sensitivity and wider linear range comparing to other reported biosensors for AβO (Li et al., 2012; Liu et al., 2017).

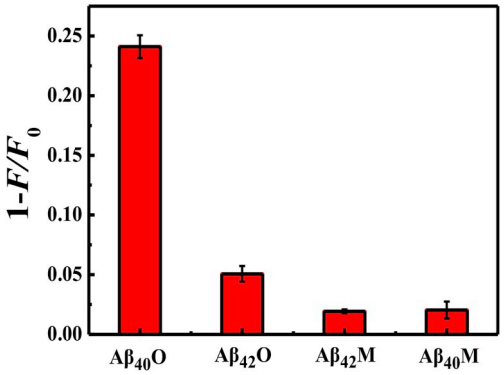

Fig. 5. Selectivity of the dsDNA2/GO-based aptasensor for $A\beta_{40}O$. The error bars mean the standard deviation for four detections ($n = 4$).

To further prove the advantage of dsDNA2/GO for improving the performance of this biosensor, we also performed the calibration curve of $A\beta_{40}O$ using dsDNA1/GO as probe, as shown in Fig. 4B (curve b). A linear equation was obtained as 1-(F/F_0) = 0.00096 $c_{A\beta40O}$ + 0.1237 ($R = 0.9916$) with a linear range from 25 to 200 nM, and the detectable lowest concentration of 25 nM.

Comparing the performance of dsDNA2/GO with that of dsDNA1/GO, it is elucidated that the higher sensitivity and wide linear rang can be simply achieved optimizing the mismatched bases of dsDNA, which is greatly crucial for the detection of low $A\beta_{40}O$ concentrations, providing an important characteristic in the development of aptsensor's applications in AD diagnosis.

3.7. Selectivity, recovery

To access the specificity of this proposed sensor, $A\beta_{40}M$, $A\beta_{42}M$ and $A\beta_{42}O$ were chosen as interfering specimens for $A\beta_{40}O$ determination. In a typical experiment, dsDNA2/GO was incubated with 1 μM $A\beta_{40}M$, 1 μM $A\beta_{42}M$ and 1 μM $A\beta_{42}O$, and 20 nM $A\beta_{40}O$, respectively. As shown in Fig. 5, although the concentrations of interfering species ($A\beta_{40}M$, $A\beta_{42}M$ and $A\beta_{42}O$) were higher than that of $A\beta_{40}O$, the fluorescent

Table 1
The detection of $A\beta_{40}O$ in CSF samples from healthy and AD patients.

CSF sample	No.	Detection amount (nM)	RSD (%)
Healthy persons	1	–	–
	2	–	–
	3	–	–
AD patients	1	9.71	4.5
	2	15.62	6.8
	3	11.36	5.6

responses resulted from interfering species were obviously lower than that caused by $A\beta_{40}O$. It demonstrates that this proposed sensor for $A\beta_{40}O$ possesses high specificity.

To estimate the reliability and applicability of this present biosensor, the recovery tests for various concentrations of $A\beta_{40}O$ have been performed in ACSF samples. As shown in Table S2, recovery rate of 0.1, 2.0 and 20 nM $A\beta_{40}O$ were 97.3%, 106.0% and 103.4%, respectively. These results demonstrate that the detection accuracy of this proposed method is acceptable and practical.

3.8. Applicability

We assessed this sensor's practical applicability in real CSF samples by measuring $A\beta_{40}O$ concentrations in CSF samples of AD patients and healthy persons, as displayed in Table 1. The concentrations of $A\beta_{40}O$ in AD patients' CSF were at the nanomolar level, while no $A\beta_{40}O$ in healthy persons' CSF was detected. This demonstrates the concentrations of $A\beta_{40}O$ in AD patients' CSF are higher than those in healthy persons' CSF, which is consistent with reports in literatures (Englund et al., 2007; Mroczko et al., 2018). Although the data for three samples is limited, the work demonstrates that it is possible to distinguish patients from healthy people by improving the sensitivity of the biosensor for AD biomarkers.

4. Conclusions

In summary, a fluorescent aptasensor for $A\beta_{40}O$ was simply fabricated based on dsDNA/GO sensing devices. bDNA containing $Apt_{A\beta}$, and cDNAs complementary to bDNA were involved, which were hybridized on GO surface to obtain dsDNA/GO sensing probe for $A\beta_{40}O$ detection. High sensitivity and specificity of the biosensor were achieved by both optimizing the number of mismatched base pairs of dsDNAand covalently binding $Apt_{A\beta}$ onto GO surface. The higher detection sensitivity was greatly improved with the lowest detectable concentration of 0.1 nM and a wider linear range from 0.1 nM to 40 nM was generated compared to previous reports. The excellent performance made it possible to detect the low concentration of AβO in CSF. It provides a rapid (response time of 30 min), simple, high sensitive and selective, and applicable method to detect the low concentrations of AβO, which is meaningful and important to distinguish AD patients from healthy persons at the early stage of disease.

Declaration of competing interest

The authors declare that they have no known competing financial interests or personal relationships that could have appeared to influence the work reported in this paper.

CRediT authorship contribution statement

Yana Zhao: Writing - original draft, Supervision. **Xin Li:** Supervision. **Yuan Yang:** Writing - review & editing. **Shihui Si:** Supervision. **Chunyan Deng:** Supervision, Supervision. **Huiyun Wu:** Supervision.

Acknowledgements

This work was financially supported by the National Natural Science Foundation of China (21727810, 21573290, 21273288).

Appendix A. Supplementary data

Supplementary data to this article can be found online at https://doi.org/10.1016/j.bios.2019.111840.

References

Baker, B.R., Lai, R.Y., Wood, M.S., Doctor, E.H., Heeger, A.J., Plaxco, K.W., 2006. J. Am. Chem. Soc. 128, 3138–3139.
Bruggink, K.A., Jongbloed, W., Biemans, E.A.L.M., Veerhuis, R., Claassen, J.A.H.R., Kuiperij, H.B., Verbeek, M.M., 2013. Anal. Biochem. 433, 112–120.
Chang, H., Tang, L., Wang, Y., Jiang, J., Li, J., 2010. Anal. Chem. 82, 2341–2346.
Deng, C., Chen, J., Nie, L., Nie, Z., Yao, S., 2009. Anal. Chem. 81, 9972–9978.
Deng, C., Liu, H., Zhang, M., Deng, H., Lei, C., Shen, L., Jiao, B., Tu, Q., Jin, Y., De Sousa, M., Martins, C.H.Z., Franqui, L.S., Fonseca, L.C., Delite, F.S., Lanzoni, E.M., Alves, O.L., 2018. J. Mater. Chem. B 6, 2803–2812.
Ellington, A.D., Szostak, J.W., 1990. Nature 346, 818–822.
Englund, H., Sehlin, D., Johansson, A.S., Nilsson, L.N.G., Gellerfors, P., Playlie, S., Lannfelt, L., Pettersson, F.E., 2007. J. Neurochem. 103, 334–345.
Felismina, T.C., Moreira, M., Goreti, F.S., 2017. Sens. Actuators, B 240, 229–238.
Fukuta, T., Nitta, A., Itoh, A., Furukawa, S., Nabeshima, T., 2001. J. Neural Transm. 108, 221–230.
Geng, J., Li, M., Ren, J., Wang, E., Qu, X., 2011. Angew. Chem. Int. Ed. 50, 4184.
Guerrini, L., Arenal, R., Mannini, B., Chiti, F., Pini, R., Matteini, P., Alvarez-Puebla, R.A., 2015. ACS Appl. Mater. Interfaces 7, 9420–9428.
Hanson, O., Zetterberg, H., Buchhave, P., Londos, E., Blennow, K., Minthon, L., 2006. Lancet Neurol. 5, 228–234.
Hallikainen, I., Koivisto, A.M., Paajanen, T., Hiltunen, A., Karppi, P., Vanhanen, M., Välimäki, T., Herukka, S.K., Soininen, H., Hänninen, T., 2012. Dement. Geriatr. Cognit. Disord. 2, 209–218.
He, S., Song, B., Li, D., Zhu, C., Qi, W., Wen, Y., Wang, L., Song, S., Fang, H., Fan, C., 2010. Adv. Funct. Mater. 20, 453–459.
He, Y., Lin, Y., Tang, H., Pang, D., 2012. Nanoscale 4, 2054–2059.
Huang, J., Wang, Z., Kim, J.-K., Su, X., Li, Z., 2015. Anal. Chem. 87, 12254–12261.
Hummers, W.S., Offeman, R.E., 1958. J. Am. Chem. Soc. 80, 1339.
Jakob-Roetne, R., Jacobsen, H., 2009. Angew. Chem. Int. Ed. 48, 3030–3059.
Li, D.Y., He, X.W., Chen, Y., Li, W.Y., Zhang, Y.K., 2013. ACS Appl. Mater. Interfaces 5, 12609–12616.
Li, H., Cao, Y., Wu, X.L., Ye, Z.H., Li, G.X., 2012. Talanta 93, 358–363.
Liu, L., Chang, Y., Yu, J., Jiang, M.S., Xia, N., 2017. Sens. Actuators, B 251, 359–365.
Liu, Z., Chen, S., Liu, B., Wu, J., Zhou, Y., He, L., Ding, J., Liu, J., 2014. Anal. Chem. 86, 12229–12235.
Lu, S., Wang, S., Zhao, J., Sun, J., Yang, X., 2017. Anal. Chem. 89, 8429–8436.
Mroczko, B., Groblewska, M., Litman-Zawadzka, A., Kornhuber, J., Lewczuk, P., 2018. J. Neural Transm. 125, 177–191.
Mukhopadhyay, R., 2005. Anal. Chem. 77, 114A–118A.
Perrin, R.J., Fagan, A.M., Holtzman, D.M., 2009. Nature 461, 916–922.
Robertson, D.L., Joyce, G.F., 1990. Nature 344, 467–468.
Rushworth, J.V., Ahmed, A., Griffiths, H.H., Pollock, N.M., Hooper, N.M., Millner, P.A., 2014. Biosens. Bioelectron. 56, 83–90.
Small, D.H., Cappai, R., 2006. J. Neurochem. 99, 708–710.
Stopschinski, B.E., Diamond, M.I., 2017. Lancet Neurol. 16, 323–332.
Swathi, R.S., Sebastian, K.L., 2009. J. Chem. Phys. 130, 086101.
Taylor, G., Freed, D.L., 1976. Nature 259, 237–239.
Taylor, M., Moore, S., Mayes, J., Parkin, E., Beeg, M., Canovi, M., Gobbi, M., Mann, D.M. A., Allsop, D., 2010. Biochemistry 49, 3261–3272.
Xia, N., Liu, L., Harrington, M.G., Wang, J.X., Zhou, F.M., 2010. Anal. Chem. 82, 10151–10157.
Xia, W., Yang, T., Shankar, G., Smith, I.M., Shen, Y., Walsh, D.M., Selkoe, D.J., 2009. Arch. Neurol. 66, 190–199.
Xiao, Y., Piorek, B.D., Plaxco, K.W., Heeger, A.J., 2005. J. Am. Chem. Soc. 127, 17990–17991.
Yamada, K., Tanaka, T., Mamiya, T., Shiotaniet, T., Kameyama, T., Nabeshima, T., 1999. Br. J. Pharmacol. 126, 235–244.
Yang, T., Li, S.M., Xu, H.X., Walsh, D.M., Selkoe, D.J., 2017. J. Neurosci. 37, 152–163.
Yi, X., Feng, C., Hu, S., Li, H., Wang, J., 2015. Analyst 141, 331–336.
Yin, Z., Wang, S., Shen, B., Deng, C., Tu, Q., Jin, Y., Shen, L., Jiao, B., Xiang, J., 2019. Anal. Chem. 91, 3539–3545.
Yu, J., He, S., Shao, C., Zhao, H., Li, J., Tian, L., 2018. Nanoscale 10, 7067–7076.
Zhao, T., Liu, R., Ding, X., Zhao, J., Yu, H., Wang, L., Xu, Q., Wang, X., Lou, X., 2018. J. Mater. Chem. B 6, 2803–2812.